

# ASRC Aerospace Corporation

P.O. Box 21087  
Kennedy Space Center, Florida 32815-0087

SBA Section 8(a) Company  
Alaska Native Corporation

NIAC CP 04-01  
Phase I  
Advanced Aeronautical/Space Concept Studies

*Analysis of a Lunar Base Electrostatic Radiation Shield Concept*

## Mid-Term Phase I Report

Charles R. Buhler, Principal Investigator  
(321) 867-4861  
Fax: (321) 867-4489  
[Charles.Buhler-1@ksc.nasa.gov](mailto:Charles.Buhler-1@ksc.nasa.gov)

Leon Wichmann, Contracting Officer  
(321) 867-1504  
Fax: (321) 867-1087  
[Leon.Wichmann-1@ksc.nasa.gov](mailto:Leon.Wichmann-1@ksc.nasa.gov)

December 15, 2004

## Introduction

*Space weather* can be defined as the total ensemble of radiation in space, as well as on the surface of moons and asteroids. It consists of electromagnetic, charged-particle, and neutral particle radiation.

The fundamental goal behind this NIAC Phase I research is to investigate methods of generating a static electric-field potential  $\Phi(x, y, z)$  in the volume above and around a “safe” or protected area on the lunar surface so that trajectories of harmful charged particle radiation are modified (deflected or reflected), thus creating a shadow over that region. Since the charged particles are not neutralized but merely redirected, there will be areas outside of the shadowed protected region that will have a higher flux concentration of radiation.

One of the fundamental limitations of the static electric (electrostatic)-field approach to radiation shielding is that complete shadowing is accomplished only by complete reflection, which can only occur for shield voltages greater than or equal to the kinetic energy (in electron volts) of the incoming charged particles. Just as habitats on Earth are protected from severe weather events and conditions, such as extreme temperatures, high winds, and UV radiation, using multiple methods of *shielding* protection from severe space weather will undoubtedly require multiple strategies. The electrostatic shield concept may be one of many methods employed to protect astronaut habitats on the lunar surface from some of the harmful effects of space weather.

## Two Design Concepts: Electrostatic Spheres and Electrostatic Screens

The goal of this Phase I award is to investigate electrostatic field configurations and methods of generating those fields that will reduce the intensity of charged-particle radiation on the lunar surface in a protected volume. A major design challenge in this approach is the requirement to shield both negative and positive particles. Complete shadowing of radiation (total reflection) is the ideal goal, but partial reduction in radiation flux may also be useful if the electrostatic shield is one component of a multistage radiation protection system.

Two parallel design activities have been pursued concurrently during the first half of Phase I.

### ELECTROSTATIC SPHERES

The motivation behind this approach is that generation of an arbitrarily specified electrostatic field can be approximated by a system of conducting spheres of specific voltages and diameters. A distinct advantage of computing the 3-D electrostatic-field potential from a system of conducting spheres is that direct analytical methods can be used, thus significantly reducing the computation complexity.

A close analogy exists to this design methodology in the field of audio engineering: a *parametric equalizer* is used to approximate a user-defined frequency response  $H(\omega)$  by summing the individual responses of second-order band pass filters of variable bandwidth, center frequency, and amplitude. If the electrostatic-field potential  $\Phi(x, y, z)$  is plotted along a line defined by the parameter  $s$ ,  $\Phi(As + a, Bs + b, Cs + c)$ , the resulting plot of  $\Phi(s)$  versus  $s$  would look similar to a plot of  $H(\omega)$  versus  $\omega$ . Well-known design techniques of finding optimized parametric filter parameters exist in order to approximate a user-defined frequency response.

Similar mathematical optimization techniques could be applied to finding the best-fit electrostatic-sphere parameters that match a desired 3-D potential contour in the radiation shield design problem. This may be an area of future work, but in this present activity, most of the

effort was devoted to generating and testing software to calculate the potential field and perform Monte Carlo simulation of charged-particle trajectories, with and without the powered spheres. The design configurations of Phase I have been based on empirical and best-guess methods of specifying the sphere parameters. Details of this method are discussed in Appendix A.

## ELECTROSTATIC SCREENS

A finite-element approach prevents us from falling into the trap of advocating a design solution simply because it is easy to calculate. Field Precision (New Mexico), our Phase I collaborator, has developed a suite of software modules to compute electric fields, magnetic fields, and charged-particle trajectory analysis, based on finite-element modeling. Field Precision is using its software to investigate a second method of radiation shielding based on electrostatic screens. Details of this method are discussed in Appendix B.

### Electrostatic Shield Design Problems and Constraints

The electrostatic shield is composed of conducting surfaces (or electrodes), connected by insulating components, and mechanical support structures. The shield may be composed of spheres, screens, combinations of the two, or something else. The goal is to find the best overall solution for creating an ideal static electric-field potential, based on electrical, mechanical, and structural engineering, as well as economic constraints. Two parts to this problem are difficult to separate: (1) define the ideal electrostatic field for radiation shielding, and (2) find a way to generate it.

Assuming that generators can be fabricated that produce the necessary voltages to power the electrostatic radiation shield, the fundamental design constraints of the system that must be considered are:

- Insulating structures, such as supports, cables, and poles, must be limited to an electric-field strength exposure of no more than some maximum value,  $E_{VB}$  in order to avoid vacuum breakdown. A conservative value for this maximum might be  $2.5 \text{ [MV m}^{-1}\text{]}$ .
- Sunlight-generated electron photoemission from the lunar surface must be blocked from interfering with the shield.
- Lunar dust must be blocked from contacting with the shield's charged surfaces.
- Charged-particle radiation from the horizon will most likely not be stopped by any practical shield configuration—a wall of lunar sand bags around the base may be a good solution.
- Attractive and repulsive coulomb forces between spheres, electrodes, and all other high-voltage structures must be balanced by appropriate mechanical support structures.
- Size and mass of deployable structures must be limited to what can be assembled by astronauts on the lunar surface.

### Shield Efficiency and Total Radiation Dosage Reduction

For the purposes of radiation shield analysis, it is useful to construct a model quantifying the dosage rate of harmful radiation received by an unprotected astronaut on the lunar surface (or in deep space). This can be empirically modeled as:

$$D_0(t) \equiv \int_0^{\infty} \rho(E,t) \beta(E) dE \quad (1)$$

where  $\rho(E,t)$  is the number density of charged particles that intersect a critical surface, or *protected region*. This critical surface could correspond to the entire surface of an astronaut's body or some other arbitrary surface surrounding the astronaut's habitat. The double integral of  $\rho(E,t)$  over all energies  $E$  and time  $t$ , gives the total number of particles  $n_0$ , a dimensionless quantity, intersecting the critical surface.

In order to estimate the biological damage from a particle of energy  $E$ , a damage coefficient  $\beta(E)$  can be used to approximate this effect. The many simplifying assumptions called upon here include ignoring the particle angle of incidence, atomic mass of the particle and composition, charge of the particle, and specific region of the body impacted by the radiation. The only parameter used in this simplified model is the particle kinetic energy,  $E$ .  $\beta(E)$  is the relative amount of biological radiation damage as a function of energy.  $\beta(E)$  may be expressed as a polynomial series, a power-law, or some other approximation function.

A shielding efficiency  $\varepsilon(E)$  can be defined (see Figure 10 of Appendix B) so that the total dosage rate of harmful radiation is reduced as described by the following integral:

$$D(t) \equiv \int_0^{\infty} [1 - \varepsilon(E)] \rho(E,t) \beta(E) dE \quad (2)$$

For a shield of perfect efficiency (i.e.,  $\varepsilon(E) = 1$ ) for all  $E$ ,  $D(t) = 0$ , according to Equation (2). Realistically, the fraction of accumulated harmful radiation dosage can be expressed as the ratio of the time integrals of Equations (1) and (2):

$$f_D \equiv \frac{\int D(t) dt}{\int D_0(t) dt} \quad \xi_D \equiv 1 - f_D \quad (3)$$

where we define  $\xi_D$  as the *dosage attenuation efficiency*. In the case of a specific flux of radiation intersecting a critical surface, the *specific efficiency*  $\xi_S$  can be defined by calculating the total number of intersecting particles with ( $n_S$ ) and without ( $n_0$ ) the shield:

$$\begin{aligned} \xi_S &\equiv 1 - \frac{\iint [1 - \varepsilon(E)] \rho(E,t) dE dt}{\iint \rho(E,t) dE dt} \\ &= 1 - \frac{n_S}{n_0} \end{aligned} \quad (4)$$

The specific efficiency  $\xi_S$  of Equation (4) will generally show a more optimistic quantity when compared to the fraction of accumulated radiation dosage  $\xi_D$  since  $\beta(E)$  would be expected to increase with energy. Only in the special (and unrealistic) case of  $\beta(E) = 1$ , would  $\xi_D = \xi_S$ , but normally,  $\xi_D < \xi_S$ .

## Future Work

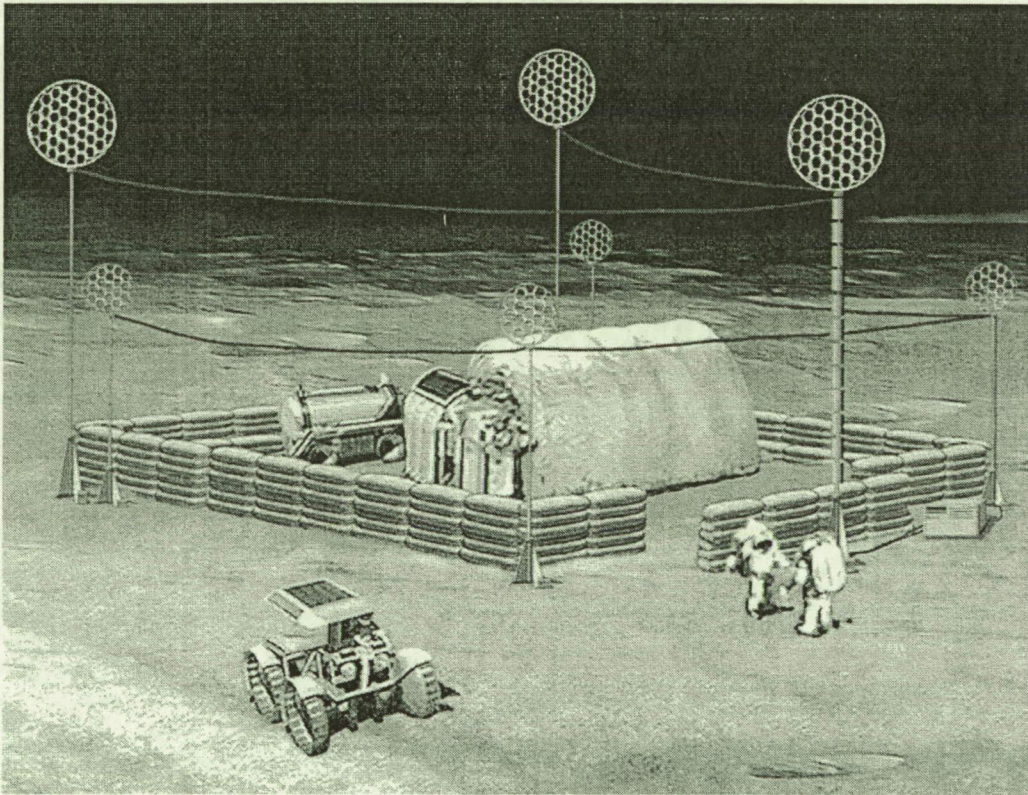
Topics for future work are listed below. Some of these topics may be appropriate as part of a possible Phase II, whereas other topics listed will be completed during Phase I.

- Future simulations will consider both a *ground shield* for protection against lunar surface dust and photoemission electrons, as well as an outer *electron shield* to deflect incoming electron radiation from space. It may be possible to combine the negative shield and the ground shield into one structure.
- A combination of screens (concept #2 – Appendix B) and spheres (concept #1 – Appendix A) may be advantages. For example, the negative ground shield would be composed of an electrostatic screen, whereas the high-voltage shield would be a set of +100 MV spheres on 40-meter poles.
- Electrostatic rings or “donuts” have been suggested. These could be configured numerous ways, such as concentrically, forming a cone over the protected area.
- The big challenge with the electrostatic-shield approach is the incredibly large voltages (an order of magnitude larger than anything obtained to date) needed to deflect ionized space radiation. Future work will investigate a concept to reduce the “base” field strength by using small transverse magnetic steering fields. The electrostatic shield works somewhat like a cathode ray tube (CRT), where the anode is analogous to the shield and where the cathode generates the radiation source. In the case of the electrostatic shield, the anode is meant to deflect oncoming charges particles. A CRT incorporates low-current magnetic steering fields. The goal of this activity is to investigate the possibility of applying the magnetic steering field concept to the electrostatic shield in order to reduce the large electric fields needed.

## Appendix A: Electrostatic Sphere Concept

The following report describes a FORTRAN simulation model, originally developed at Kennedy Space Center, NASA Applied Physics Lab (2002 to 2003), for modeling charged-particle radiation scattering from electrostatic spheres. This report describes the mathematical details, based primarily on modeling the dynamics of a charged particle in an electric field. The particle velocity is determined using relativistic mechanics, from user specified kinetic energy distributions. The primary modifications made to that software for the NIAC Phase I project are as follows:

- Incorporated a zero-potential ground plane, representing the lunar surface, using image charges below the surface.
- Incorporated a hemisphere isotropic radiation trajectory distribution, representing the lunar sky.
- Incorporated two particle Monte Carlo energy distributions, for two independent particles of arbitrary mass and charge. This allows simultaneous study of electron and positive-ion radiation.



The above concept artwork depicts an electrostatic-sphere-based radiation shield. In this example, the lower *ground shield* is at a medium voltage potential (approximately -100 kV), prevents electrons from space from reaching the surface, and prevents electrons from the surface from reaching the upper high-voltage spheres. The walls, composed of bagged lunar regolith, stop charged particles from the horizon. Note that this figure is for conceptual purposes only and does not necessarily scale properly. For example, if the high-voltage spheres were at +100 MV, then the poles would need to be 40 meters high to satisfy the constraint that maximum fields are kept below the vacuum breakdown value of  $2.5 \text{ MV m}^{-1}$ .

Figures 3 through 6, following the Appendix A report, are simulations of a complex sphere configuration consisting of seven upper negatively charged spheres and three smaller positively charged spheres. The protected region is arbitrarily defined as a hemisphere of 4-meter radius at  $x = 0, y = 0, z = 0$  (on the lunar surface). The software generates 10,000 particles, half of which are 50-MeV protons and half are 5-MeV electrons. The first of each set of figures show the simulation results with zero shield voltage (i.e., no external electric fields). This provides a comparison to powered shield shown as the second figure of each set. For this particular simulation example, the number of particles that intersect the *protected region* in the unpowered case is  $N_{off} = 323$  and  $N_{on} = 20$  in the powered case. Therefore, specific shield efficiency  $\xi_s$  from Equation (4) can be written as

$$\xi_s = 1 - \frac{N_{on}}{N_{off}} \quad (\text{A-1})$$

In the case of this simulation,  $\xi_s = 0.94$  or 94 percent.

# NIAC Phase I: Lunar Electrostatic Shield Model (LESM)

## *Isotropic Radiation with Relativistic Particles Velocities, Spheres with First Order Image Charge Correction, and Semi-Sphere Option*

ASRC Aerospace.  
Kennedy Space Center, FL 32899

November 18, 2004

*Version 1.1*

THE ELECTRIC FIELD due to a system of  $N$  point charges at a field point  $\mathbf{r}$  is given by:

$$\mathbf{E}(\mathbf{r}) = \frac{1}{4\pi\epsilon_0} \sum_{i=1}^N q_i \frac{\mathbf{r} - \mathbf{r}_i}{|\mathbf{r} - \mathbf{r}_i|^3} \quad (1)$$

where  $\mathbf{r}_i$  is the location of the  $i$ th point charge  $q_i$ . If the  $i$ th point charge is implemented as a sphere with radius  $R_i$  and a *uniform charge distribution* at potential  $V_i$ , Equation (1) can be rewritten as:

$$\mathbf{E}(\mathbf{r}) = \sum_{i=1}^N V_i R_i \frac{\mathbf{r} - \mathbf{r}_i}{|\mathbf{r} - \mathbf{r}_i|^3} \quad (2)$$

THE TRAJECTORY of a charged particle of rest mass  $m_0$  and charge  $Q$  in the electric field given by Equation (1) is determined by its equation of motion:

$$\begin{aligned} Q\mathbf{E}(\mathbf{r}) &= \dot{\mathbf{p}} = \frac{d}{dt}(\gamma m_0 \mathbf{v}) \\ &= \gamma m_0 \left( \dot{\mathbf{v}} + \gamma^2 \frac{\mathbf{v} \cdot \dot{\mathbf{v}}}{c^2} \mathbf{v} \right) \end{aligned} \quad (3)$$

where  $\gamma \equiv (1 - v^2/c^2)^{-1/2}$ .

The acceleration of the particle,  $\mathbf{a} \equiv \dot{\mathbf{v}}$ , of the particle is calculated by re-writing Equation (3) as:

$$\mathbf{C} \cdot \mathbf{a} = \frac{Q}{\gamma m_0} \mathbf{E}(\mathbf{r}) \quad (4)$$

where,

$$\mathbf{C} = \begin{pmatrix} c_{11} & c_{12} & c_{13} \\ c_{21} & c_{22} & c_{23} \\ c_{31} & c_{32} & c_{33} \end{pmatrix} = \begin{pmatrix} 1 + \gamma^2 \frac{v_x^2}{c^2} & \gamma^2 \frac{v_x v_y}{c^2} & \gamma^2 \frac{v_x v_z}{c^2} \\ \gamma^2 \frac{v_y v_x}{c^2} & 1 + \gamma^2 \frac{v_y^2}{c^2} & \gamma^2 \frac{v_y v_z}{c^2} \\ \gamma^2 \frac{v_z v_x}{c^2} & \gamma^2 \frac{v_z v_y}{c^2} & 1 + \gamma^2 \frac{v_z^2}{c^2} \end{pmatrix} \quad (5)$$

Solving for  $\mathbf{a}$  in Equation (4),

$$\begin{aligned} \mathbf{a} &= \frac{Q}{\gamma m_0} \mathbf{C}^{-1} \cdot \mathbf{E}(\mathbf{r}) \\ &= \frac{1}{B} \begin{pmatrix} A_x \\ A_y \\ A_z \end{pmatrix} \end{aligned} \quad (6)$$

where,

$$B = (c_{13}c_{22}c_{31} - c_{12}c_{23}c_{31} - c_{13}c_{21}c_{32} + c_{11}c_{23}c_{32} + c_{12}c_{21}c_{33} - c_{11}c_{22}c_{33}) m_0 \gamma \quad (7)$$

and,

$$A_x = (c_{23}c_{32}E_x - c_{22}c_{33}E_x - c_{13}c_{32}E_y + c_{12}c_{33}E_y + c_{13}c_{22}E_z - c_{12}c_{23}E_z)Q \quad (8a)$$

$$A_y = (-c_{23}c_{31}E_x + c_{21}c_{33}E_x + c_{13}c_{31}E_y - c_{11}c_{33}E_y - c_{13}c_{21}E_z + c_{11}c_{23}E_z)Q \quad (8b)$$

$$A_z = (c_{22}c_{31}E_x - c_{21}c_{32}E_x - c_{12}c_{31}E_y + c_{11}c_{32}E_y + c_{12}c_{21}E_z - c_{11}c_{22}E_z)Q \quad (8c)$$

Based on a Taylor series expansion about time point  $k$ , a set of difference equations for position and velocity can be expressed as:

$$\begin{aligned} \mathbf{v}_{k+1} &\approx \mathbf{v}_k + \dot{\mathbf{v}}_k \Delta t \\ &\approx \mathbf{v}_k + \mathbf{a}_k \Delta t \end{aligned} \quad (9a)$$

$$\begin{aligned} \mathbf{r}_{k+1} &\approx \mathbf{r}_k + \dot{\mathbf{r}}_k \Delta t + \frac{1}{2} \ddot{\mathbf{r}}_k \Delta t^2 \\ &\approx \mathbf{r}_k + \mathbf{v}_k \Delta t + \frac{1}{2} \mathbf{a}_k \Delta t^2 \end{aligned} \quad (9b)$$

In the non-relativistic case, the acceleration in Equations (9) reduces to  $\mathbf{a}_k = (Q/m_0)\mathbf{E}_k$ . In the general case (non-relativistic and relativistic),  $\mathbf{a}_k$  is computed from Equation (6) using  $\mathbf{r}_k$ ,  $\mathbf{v}_k$ , and  $\mathbf{E}(\mathbf{r}_k)$ .

INITIAL STATE VECTOR of the particle is modeled by setting the initial particle position  $\mathbf{r}_0$  at a constant far field distance  $R'_0$  from the vehicle (dotted spherical surface in Figure 1), using random parameters,  $\phi'$  and  $\theta'$ . The particle's initial velocity  $\mathbf{v}_0$  is composed of an initial speed  $v_0$  and a direction. The direction of  $\mathbf{v}_0$  is given by the two random variables, as shown in Figure 1, angles  $\phi$  and  $\theta$ . The vehicle is fixed at the origin of the coordinate system and therefore the particle's initial state vector and trajectory is expressed relative to the vehicle's coordinate system. The software is configured to reject all initial states whose initial trajectory vector does not intersect with the inner sphere of radius  $R_0$ . This is determined by performing the following comparison:  $\left| \mathbf{r}_0 + R'_0 \frac{\mathbf{v}_0}{|\mathbf{v}_0|} \right| < R_0$ . If false, the trajectory is rejected and a new one is calculated.

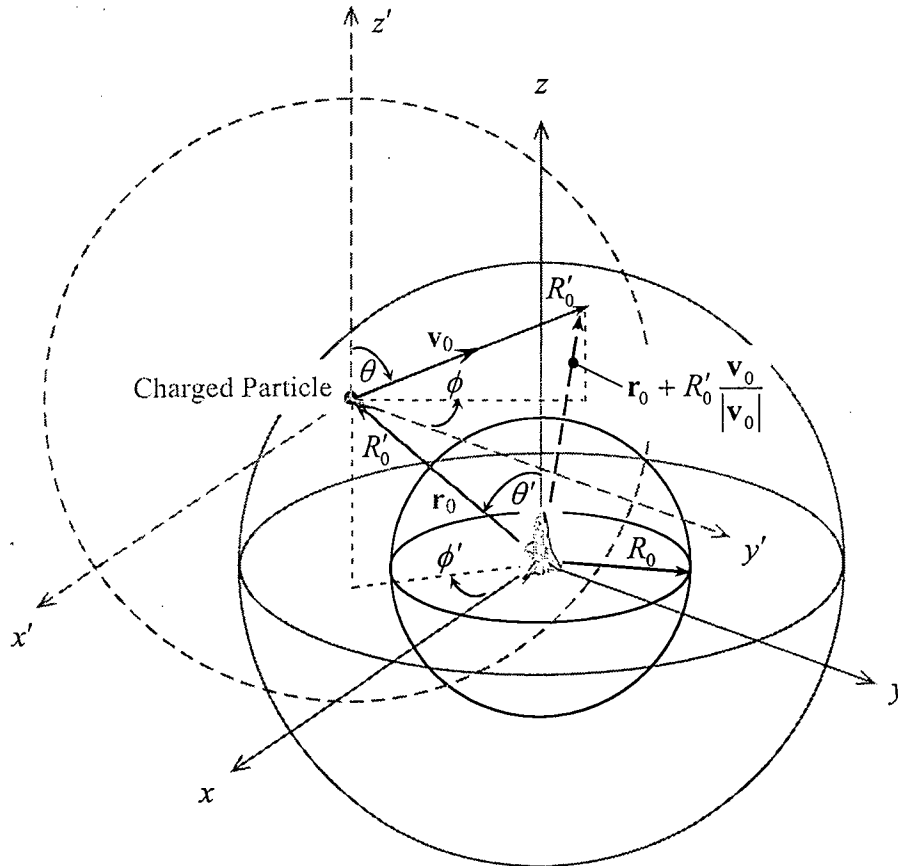


Figure 1. Diagram of Isotropic Radiation, Showing Initial State of Charged Particle.

The particle's initial velocity vector is given by the following:

$$\mathbf{v}_0 = \begin{pmatrix} v_x \\ v_y \\ v_z \end{pmatrix} = v_0 \begin{pmatrix} \alpha \\ \beta \\ \gamma \end{pmatrix} \quad (10a)$$

where,  $\alpha^2 + \beta^2 + \gamma^2 = 1$ , and:

$$\alpha \equiv \sin \theta \cos \phi \quad \beta \equiv \sin \theta \sin \phi \quad \gamma \equiv \cos \theta \quad (10b)$$

The particle's initial velocity  $\mathbf{v}_0$  does not change until the particle encounters an external force. For the purpose of simulation, it is convenient to assume that the force from the vehicle's electrostatic shield has no influence on the particle's trajectory until it is within a radius  $R'_0$  from the vehicle. The initial position vector  $\mathbf{r}_0$  is (see Figure 1):

$$\mathbf{r}_0 = R'_0 \begin{pmatrix} \sin \theta' \cos \phi' \\ \sin \theta' \sin \phi' \\ \cos \theta' \end{pmatrix} \quad (11)$$

An option has been added in version 1.0: the *semi-sphere radiation* flag which limits the radiation trajectories to the upper hemisphere, for the purpose of lunar base version.

PROBABILITY DISTRIBUTIONS of the individual model parameters are based on the *uniform* distribution  $P_U$  equal to one in the interval from 0 to +1, and zero elsewhere; a sinusoidal distribution  $P_S(u) = \sin u$  in the interval from 0 to +1, and zero elsewhere; and the *normal* distribution  $P_N$  of unit variance and zero mean, defined by:

$$P_N(u) = \frac{e^{-u^2/2}}{\sqrt{2\pi}} \quad (12a)$$

Table 1 describes the individual model parameters and their corresponding distribution functions.  $R'_0$  is the distance to the initial position of the charged particle, while  $\rho_0$  is the critical radius of influence. As shown in Figure 1, the angles  $\theta$  and  $\theta'$  describing the incoming particle velocity, range from 0 to  $\pi$ , whereas the angles  $\phi$  and  $\phi'$  range from 0 to  $2\pi$ . Note that  $R_0 < R'_0$  and  $\rho_0 < R'_0$ , however, either  $\rho_0 < R_0$  or  $\rho_0 \geq R_0$  is valid.

The speed  $v_0$  of the particle is determined from the kinetic energy,  $T$ :

$$v_0 = \frac{c\sqrt{1+2\xi}}{1+\xi} \quad \xi \equiv \frac{m_0 c^2}{T_0} \quad (13)$$

where  $m_0$  is the rest mass of the particle. The energy of the particle is determined by the standard deviation  $\sigma_E$  and mean  $T_0$ .

Table 1. Model Parameters and Associated Distributions.

Model Parameter	Associated Constant	Type of Distribution	Distribution Formula
$\rho_0$	$\rho_0$	constant	-
$R_0$	$R_0$	constant	-
$R'_0$	$R'_0$	constant	-
$\theta$	$\pi$	sinusoidal	$\pi P_S$
$\theta'$	$\pi$	sinusoidal	$\pi P_S$
$\phi$	$2\pi$	uniform	$2\pi P_U$
$\phi'$	$2\pi$	uniform	$2\pi P_U$
$T$	$\sigma_E, T_0$	normal <sup>†</sup>	$\sigma_E P_N + T_0$

<sup>†</sup> The charged particle energy distribution will be replaced with a more meaningful distribution function in future versions of the model.

If the energy of the particle is expressed in *electron volts* [eV], the speed  $v_0$  of the particle from Equation (13) is modified as:

$$\xi \equiv \frac{m_0 c^2}{q T_0} \quad (14)$$

where the mass and velocity are expressed in *mks* units, and  $q$  is the fundamental unit of charge  $\approx 1.6 \cdot 10^{-19}$  [C].

**PLOTTING OF PARTICLE TRAJECTORIES:** In order to effectively plot the particle trajectory and intersections with the critical radius sphere defined by  $\rho_0$ , three projections of the 3D volume particle paths are generated as *xyPlot*, *xzPlot*, and *yzPlot*. These plots are not as easily interpreted as the previous plots where the trajectories intersected with a disk. However, after some thought, it should be easy to understand what is occurring.

Previous versions of ESM used  $\rho_0$  as the plot scale factor, such that the plot extent both in the horizontal and vertical directions, is  $2\rho_0$ . Starting with this version ESM (v5.1), and all future versions, the plot will be scaled by a separate parameter,  $\rho_p$ , such that the plot extent will be  $2\rho_p$  in both dimensions.

IMAGE CHARGE CORRECTION applied to the system of conducting spheres, results in a configuration as depicted in Figure 2.

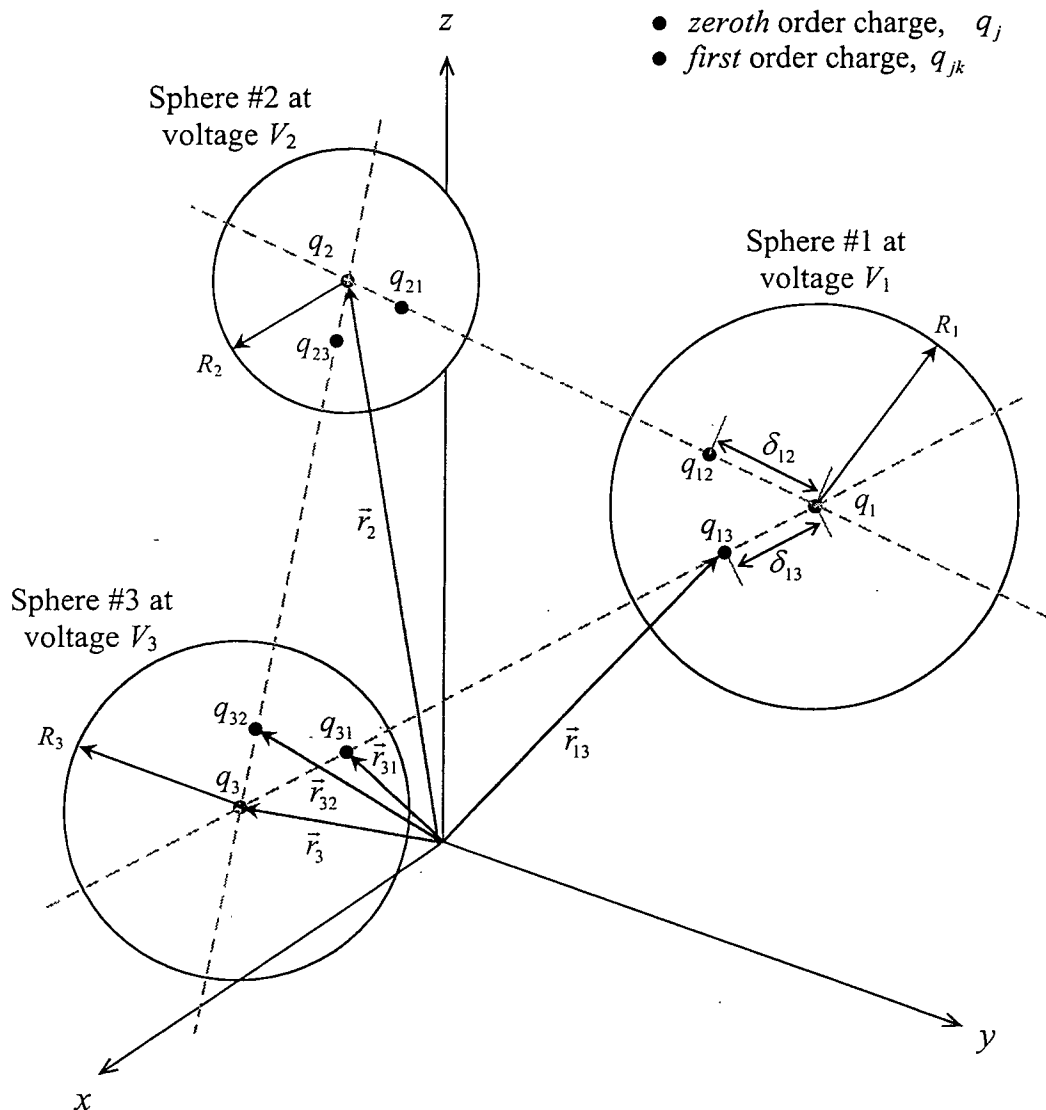


Figure 2. Image Charge Treatment of a System of Conducting Spheres.

The electric field from Equation (1) now becomes a double summation over all  $N$  spheres, where there are  $N^2$  total charges,  $N$  zeroth order charges and  $N(N-1)$  first order image charges:

$$\mathbf{E}(\mathbf{r}) = \frac{1}{4\pi\epsilon_0} \sum_{i=1}^N \left( q_i \frac{\mathbf{r} - \mathbf{r}_i}{|\mathbf{r} - \mathbf{r}_i|^3} + \sum_{\substack{j=1 \\ j \neq i}}^N q_{ij} \frac{\mathbf{r} - \mathbf{r}_{ij}}{|\mathbf{r} - \mathbf{r}_{ij}|^3} \right) \quad (15)$$

where the image charge parameters are given by the following relations:

$$q_{ij} = -\frac{R_i}{|\mathbf{r}_i - \mathbf{r}_j|} q_j \quad (16a)$$

$$\mathbf{r}_{ij} = \mathbf{r}_i - R_i \frac{\mathbf{r}_i - \mathbf{r}_j}{|\mathbf{r}_i - \mathbf{r}_j|^2} \quad (16b)$$

The potential on the surface of sphere  $k$  can be expressed as:

$$V_k = \frac{1}{4\pi\epsilon_0} \sum_{i=1}^N \left( \frac{q_i}{|R_k \mathbf{e} + \mathbf{r}_k - \mathbf{r}_i|} + \sum_{\substack{j=1 \\ j \neq i}}^N \frac{q_{ij}}{|R_k \mathbf{e} + \mathbf{r}_k - \mathbf{r}_{ij}|} \right) \quad (17)$$

where  $\mathbf{e}$  is any unit vector. Since all charges are unknowns, the goal is to eliminate all  $q$ 's from Equation (15).

$$\begin{aligned} V_k &= \frac{1}{4\pi\epsilon_0} \sum_{i=1}^N \left( \frac{q_i}{|R_k \mathbf{e} + \mathbf{r}_k - \mathbf{r}_i|} + \sum_{\substack{j=1 \\ j \neq i}}^N \frac{q_{ij}}{|R_k \mathbf{e} + \mathbf{r}_k - \mathbf{r}_{ij}|} \right) \\ &= \frac{1}{4\pi\epsilon_0} \sum_{i=1}^N \left( \frac{q_i}{|R_k \mathbf{e} + \mathbf{r}_k - \mathbf{r}_i|} - \sum_{\substack{j=1 \\ j \neq i}}^N \frac{q_j R_i}{|\mathbf{r}_i - \mathbf{r}_j| \cdot |R_k \mathbf{e} + \mathbf{r}_k - \mathbf{r}_{ij}|} \right) \\ &= \frac{1}{4\pi\epsilon_0} \sum_{i=1}^N q_i \left( \frac{1}{|R_k \mathbf{e} + \mathbf{r}_k - \mathbf{r}_i|} - \sum_{\substack{j=1 \\ j \neq i}}^N \frac{R_j}{|\mathbf{r}_j - \mathbf{r}_i| \cdot |R_k \mathbf{e} + \mathbf{r}_k - \mathbf{r}_{ji}|} \right) \\ &= \sum_{i=1}^N C_{ki} q_i \end{aligned} \quad (18a)$$

where,

$$C_{ki} \equiv \frac{1}{4\pi\epsilon_0} \left( \frac{1}{|R_k \mathbf{e} + \mathbf{r}_k - \mathbf{r}_i|} - \sum_{\substack{j=1 \\ j \neq i}}^N \frac{R_j}{|\mathbf{r}_j - \mathbf{r}_i| \cdot |R_k \mathbf{e} + \mathbf{r}_k - \mathbf{r}_{ji}|} \right) \quad (18b)$$

Equation (18a) can also be expressed in matrix form as:

$$\mathbf{V} = \mathbf{C} \cdot \mathbf{q} \quad (19a)$$

and solving for  $\mathbf{q}$ :

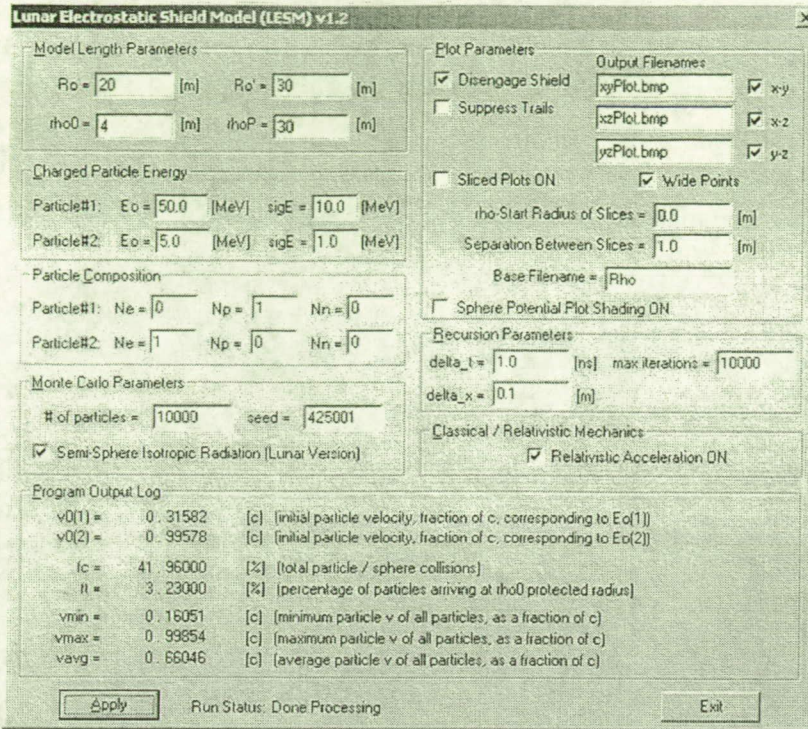
$$\mathbf{q} = \mathbf{C}^{-1} \cdot \mathbf{V} \quad (19b)$$

where  $\mathbf{V}$  is a vector of length  $N$  of sphere voltages  $V_k$ ,  $\mathbf{q}$  is a vector of length  $N$  of zeroth order charges  $q_i$ , and  $\mathbf{C}$  is an  $N \times N$  array as described by Equation (18b).

Since  $\mathbf{e}$  is a random unit vector,  $\mathbf{C}$  according to Equation (18b) will not have a unique value. A better estimate of  $\mathbf{C}$  is obtained by averaging Equation (18b) over many random unit vectors,  $\mathbf{e}_l$ :

$$C_{ki} \equiv \frac{1}{4\pi\epsilon_0} \frac{1}{M} \sum_{l=1}^M \left( \frac{1}{|R_k \mathbf{e}_l + \mathbf{r}_k - \mathbf{r}_i|} - \sum_{\substack{j=1 \\ j \neq i}}^N \frac{1}{|R_k \mathbf{e}_l + \mathbf{r}_k - \mathbf{r}_{ji}|} \cdot \frac{R_j}{|\mathbf{r}_j - \mathbf{r}_i|} \right) \quad (20)$$

The weakness of this method may be related to the ambiguous solution which is dependent on the specific choices of  $\mathbf{e}_l$  in Equation (20). As the number of values averaged over increase (i.e., as  $M$  increase), the solution given by Equation (19b) may converge to a unique value.



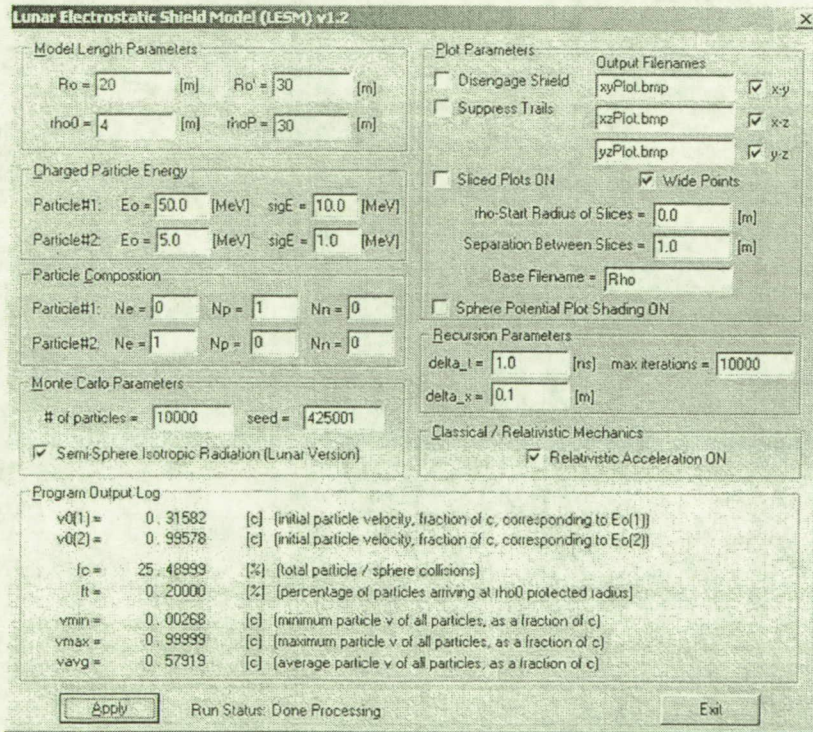
Shield OFF  
(unpowered)

Sphere Configuration File  
Shaded Entries Correspond To Image Charges Below Lunar Surface

20    Number of Spheres

V [MV]	R [m]	x [m]	y [m]	z [m]
150.0	3.0	5.0	0.0	8.0
150.0	3.0	-2.5	4.33	8.0
150.0	3.0	-2.5	-4.33	8.0
-50.0	4.0	10.0	0.0	12.0
-50.0	4.0	-5.0	8.66	12.0
-50.0	4.0	-5.0	-8.66	12.0
-50.0	5.0	0.0	0.0	16.0
-50.0	4.0	-15.0	0.0	8.0
-50.0	4.0	7.5	12.99	8.0
-50.0	4.0	7.5	-12.99	8.0
-150.0	3.0	5.0	0.0	-8.0
-150.0	3.0	-2.5	4.33	-8.0
-150.0	3.0	-2.5	-4.33	-8.0
50.0	4.0	10.0	0.0	-12.0
50.0	4.0	-5.0	8.66	-12.0
50.0	4.0	-5.0	-8.66	-12.0
50.0	5.0	0.0	0.0	-16.0
50.0	4.0	-15.0	0.0	-8.0
50.0	4.0	7.5	12.99	-8.0
50.0	4.0	7.5	-12.99	-8.0

Figure 3a. Simulation Run of Unpowered Lunar Electrostatic Shield Model (LESM v1.2) – User Interface and Sphere Configuration File.



Shield ON  
(powered)

Figure 3b. Simulation Run of Powered Lunar Electrostatic Shield Model (LESM v1.2).

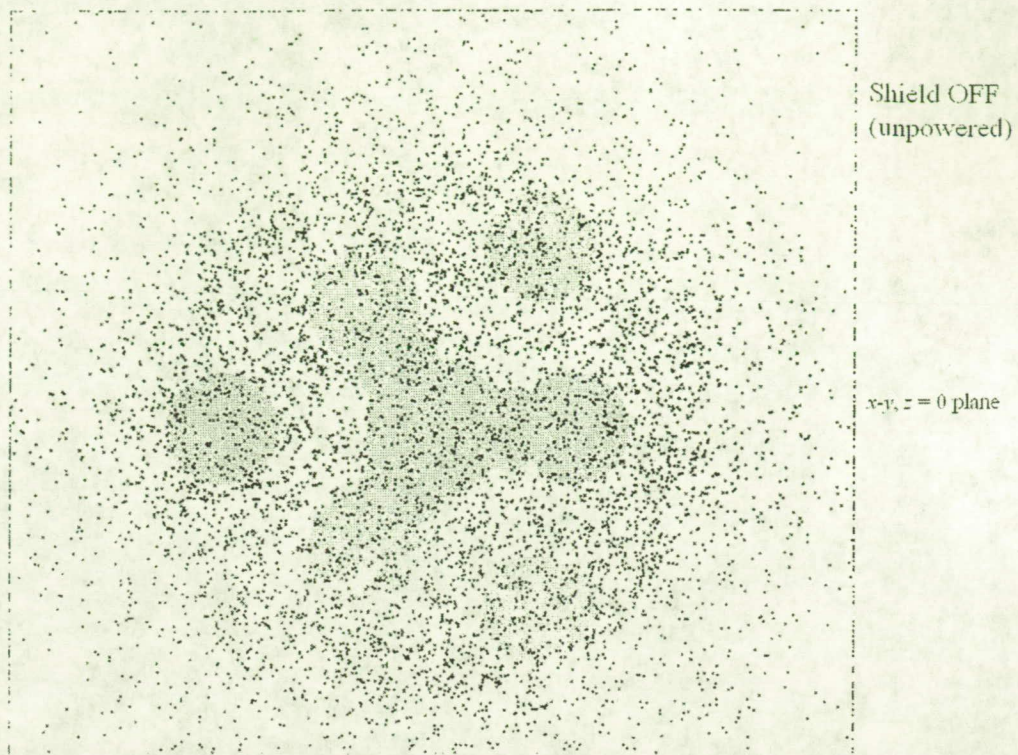


Figure 4a. Simulation Run of Lunar Electrostatic Shield Model (LESM v1.2) – Red dots are intersection of electrons and blue dots are intersection of protons with lunar surface ( $z = 0$ ). Gray circles are x-y projections of unpowered electrostatic spheres.

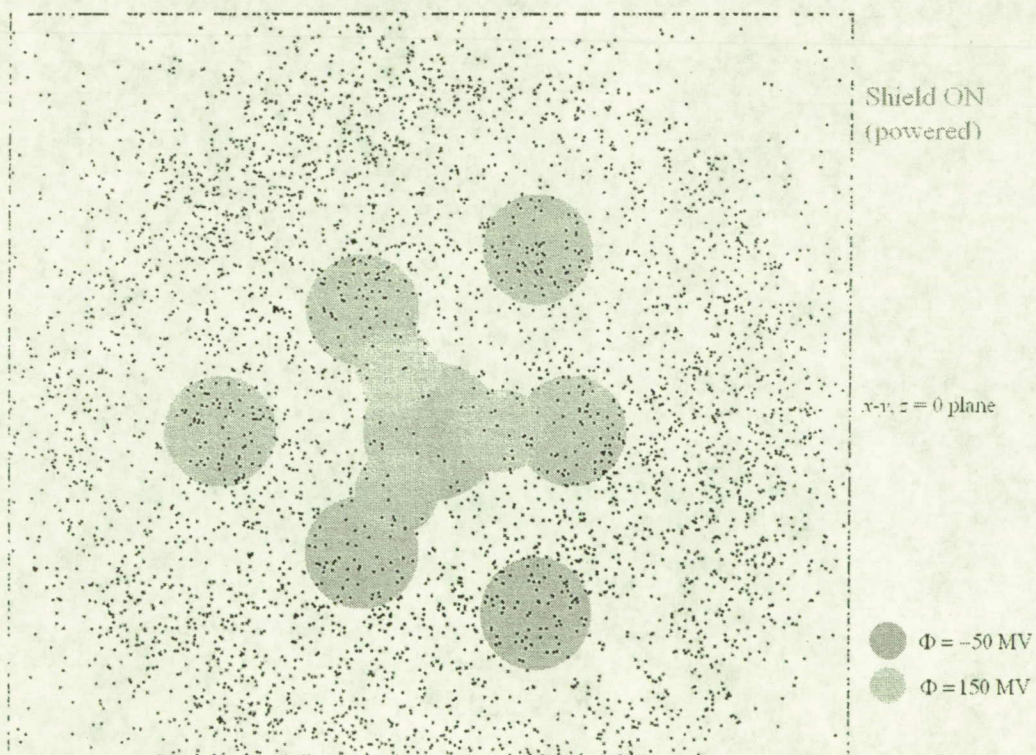


Figure 4b. Simulation Run of Lunar Electrostatic Shield Model (LESM v1.2) – Red dots are intersection of electrons and blue dots are intersection of protons with lunar surface ( $z = 0$ ). Purple and cyan circles are x-y projections of powered electrostatic spheres.

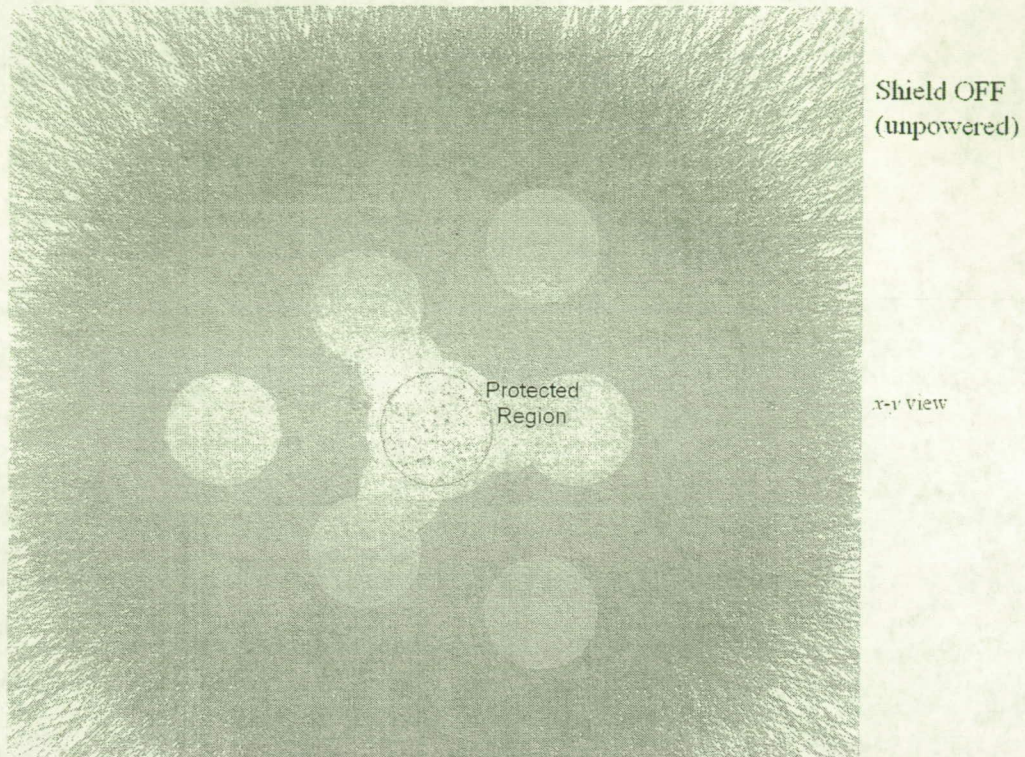


Figure 5a. Simulation Run of Lunar Electrostatic Shield Model (LESM v1.2) – Red dots are intersection of electrons and blue dots are intersection of protons with a 4 [m] radius sphere (protected area) centered at  $x = 0$ ,  $y = 0$ ,  $z = 0$ . Gray circles are x-y projections of unpowered electrostatic spheres. Yellow-gray trails are particle trajectory paths.

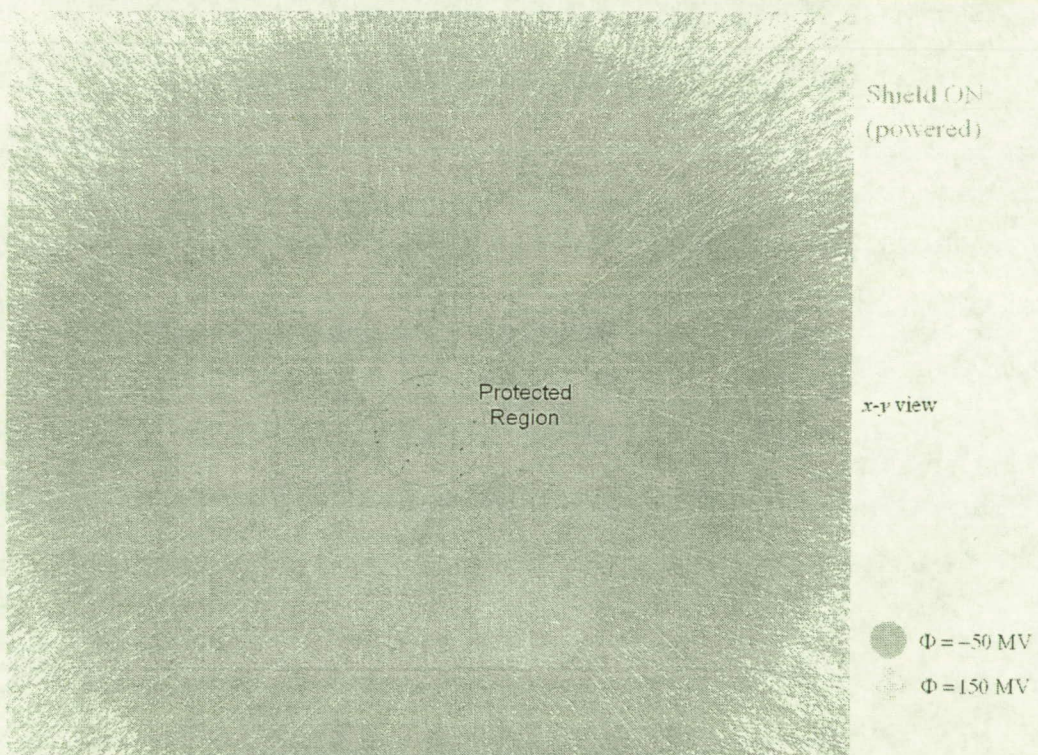


Figure 5b. Simulation Run of Lunar Electrostatic Shield Model (LESM v1.2) – Red dots are intersection of electrons and blue dots are intersection of protons with a 4 [m] radius sphere (protected area) centered at  $x = 0$ ,  $y = 0$ ,  $z = 0$ . Purple and cyan circles are x-y projections of powered electrostatic spheres. Yellow-gray trails are particle trajectory paths.

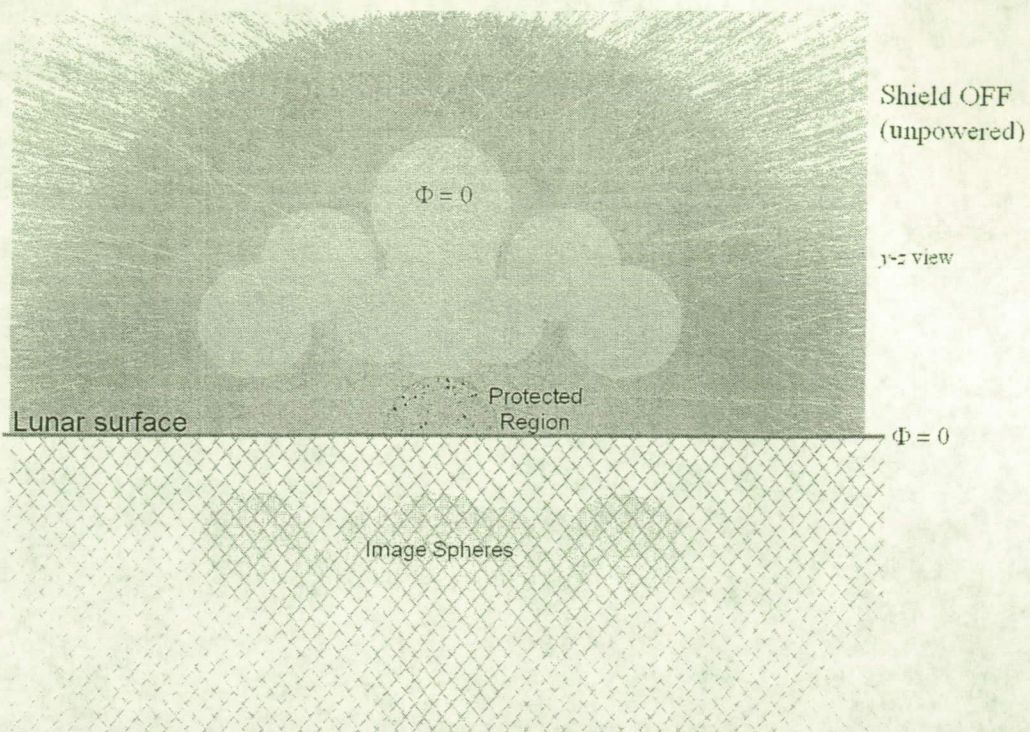


Figure 6a. Simulation Run of Lunar Electrostatic Shield Model (LESM v1.2) – Red dots are intersection of electrons and blue dots are intersection of protons with a 4 [m] radius sphere (protected area) centered at  $x = 0, y = 0, z = 0$ . Gray circles are  $y$ - $z$  projections of unpowered electrostatic spheres. Yellow-gray trails are particle trajectory paths.

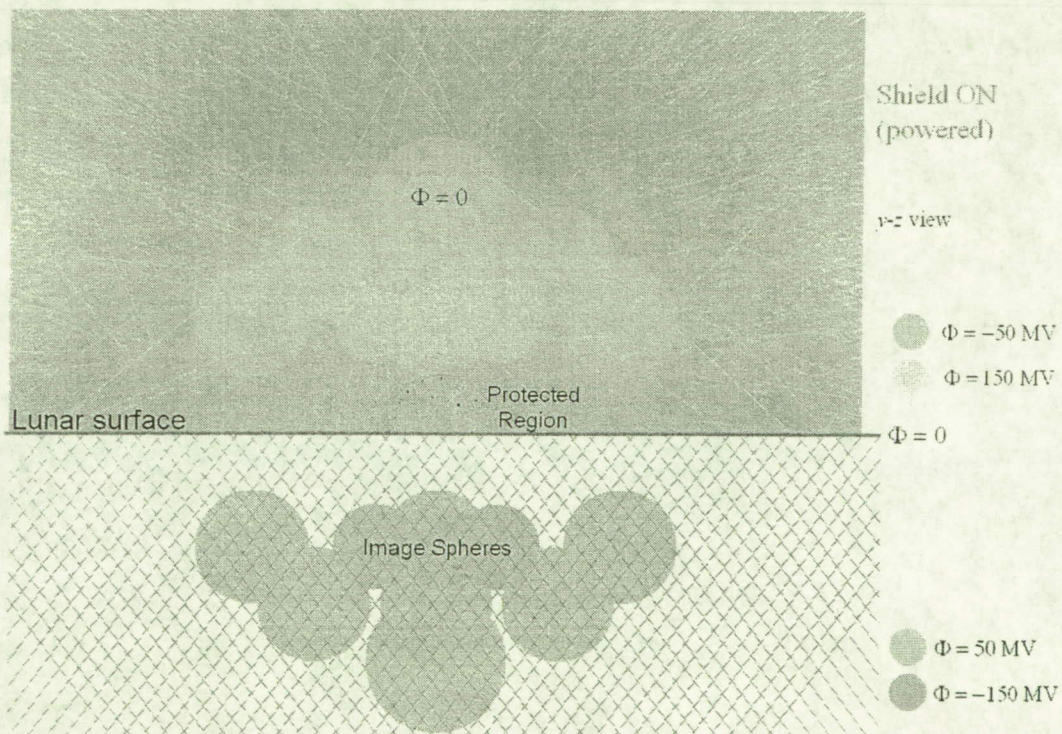


Figure 6b. Simulation Run of Lunar Electrostatic Shield Model (LESM v1.2) – Red dots are intersection of electrons and blue dots are intersection of protons with a 4 [m] radius sphere (protected area) centered at  $x = 0, y = 0, z = 0$ . Purple and cyan circles are  $y$ - $z$  projections of powered electrostatic spheres. Yellow-gray trails are particle trajectory paths.

## Appendix B: Electrostatic Screen Concept

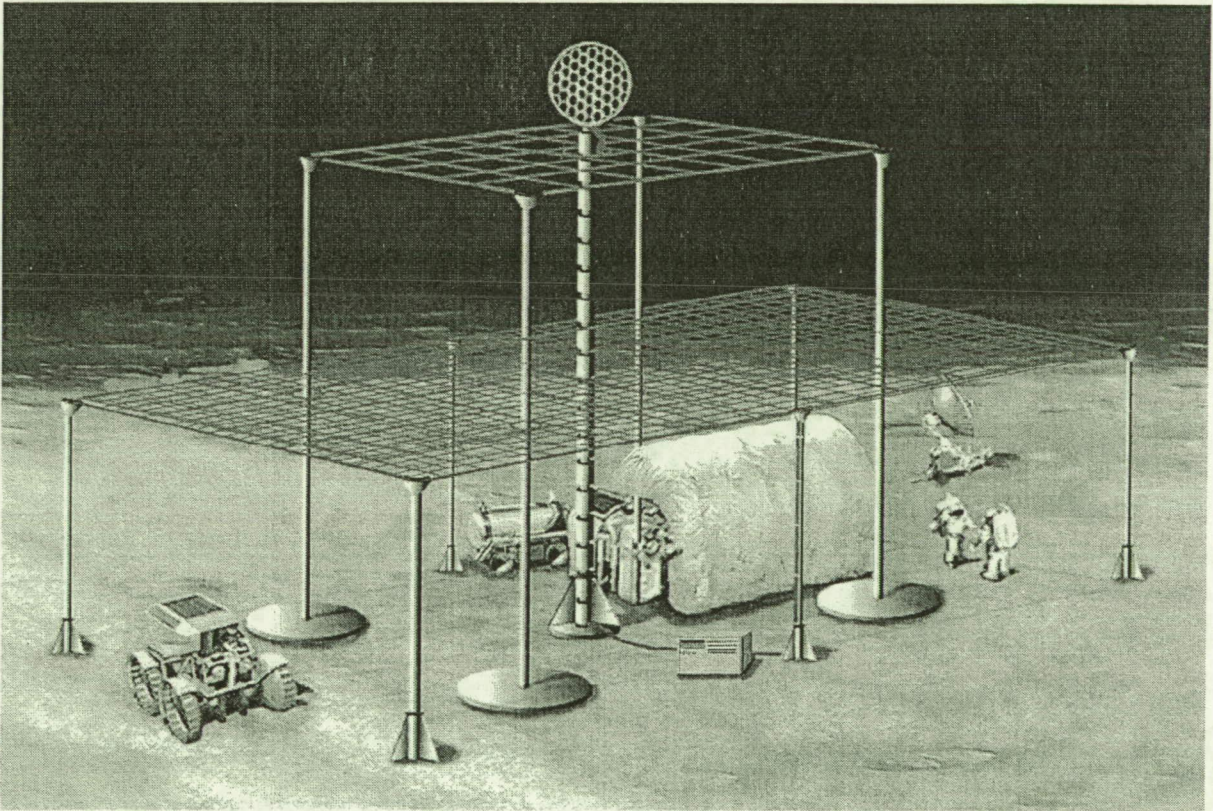
The following report is a detailed analysis of an electrostatic radiation shield design, done independently by Field Precision (New Mexico). Some of the highlights and conclusions of this report are:

- The theoretical best shielding efficiency (where the maximum is 1) goes as:

$$\varepsilon(E) = \sqrt{q\Phi_0/E} \quad (\text{B-1})$$

where  $\Phi_0$  is the maximum shield voltage,  $q$  is the charge on the particle, and  $E$  is the kinetic energy of the particle in electron volts.

- Field Precision software simulations support the conclusion that electrostatic screens provide a more efficient shielding system, one that approaches the ideal efficiency given by Equation (B-1)
- A negative ground shield is essential to stopping electron photoemission. The ground shield may also be effective at solving the lunar dust contamination problem.



The above artwork figure illustrates the electrostatic screen shield concept. Again, this figure is not to scale and comments similar to those in Appendix A apply (i.e., maximum fields must be kept below the vacuum breakdown value so that the poles would need to be 40 meters high in order to achieve a useable shielding voltage of  $\Phi_0 = 100$  MV. Also, the mesh density of the screens would be much higher than that illustrated, and the area extent of screen coverage would need to be greater in order to shield the working area shown in the figure. As with the previous sphere concept described in Appendix A, the screen configuration would not be able to stop low-elevation-angle radiation from coming in from the horizon; thus a wall would be needed for complete protection.

# Report 03

## Constraints on Electrostatic Shields for a Moon Base

Stanley Humphries  
Field Precision, Albuquerque, NM  
Prepared for ASRC Aerospace Corporation  
under Subcontract Number WFO-05-001

November 2004

### 1 Shield system concept

It is important to delineate a clear set of goals for and constraints on an electrostatic shielding system for a moon base before proceeding to an extensive program of three-dimensional simulations. To begin, I shall list several basic facts. The surface of moon is approximately an equipotential plane. In the following discussions, I shall take the surface potential as a reference (*i.e.*, ground potential equal to 0.0 V). Clearly, personnel and equipment on the moon surface must be approximately at ground potential. The potential of the infinite space above is also approximately  $\phi = 0.0$  V. Any difference in the potential of the moon surface and space would result in an exchange of low-energy electrons that would restore the balance. The issue of concern is the flux of energetic ions that arrive from space as a result of solar proton events or as part of the galactic cosmic radiation. The spatial distribution of incident ions is approximately isotropic. The role of an electrostatic shield is to reduce the energy-flux of ions that strikes a protected area on the moon surface. No matter what the electrode geometry, the basic function of the shield is to generate a region of high positive potential above the protected area that will reflect a high proportion of incident ions. Note that the shield

cannot change the average energy of non-reflected ions that are able to reach the surface. These ions start in space at the reference potential and strike objects at the same potential. I discussed a second constraint in my first report – electric field components transverse to the direction of ion motion will not change the average flux of unreflected ions if the incident distribution is isotropic. For a given applied voltage, the implication is that the most effective shield is one that maintains a uniform positive potential over the protected area. Therefore, in this report I consider sheet or mesh electrodes. Multiple electrode arrays would only yield an advantage if they had significantly smaller weight.

Figure 1 shows the preliminary concept for a moon base shield presented in our proposal. This approach has several problems:

- The electrodes over the ground plane are spaced too far apart compared to their height. The magnitude of the potential barrier at the center of the array will be only a fraction of the applied voltage on the spheres.
- The conceptual design of the high-voltage system is optimistic. The figure shows spheres on thin poles with a nearby small box to create the voltage. In actuality, each sphere would rest on a Van De Graaf generator operating at 20 MV or higher, a piece of equipment that would dwarf any of the structures on the ground. Disregarding the issue of whether a multi-MV column can operate in vacuum, the use of multiple generators would be wasteful.
- Intense electric fields on the lunar surface would polarize dust particles which would be attracted to regions of high electric field gradient.
- Personnel and equipment are not protected against strong fields, so there is a possibility of a damage or electrocution in the event of a breakdown.

The next section describes an alternate geometry that resolves the problems.

## 2 Improved shield system

Assuming that high-voltage engineering problems can be solved, Figure 2 shows an improved version of an electrostatic shield. The system utilizes a

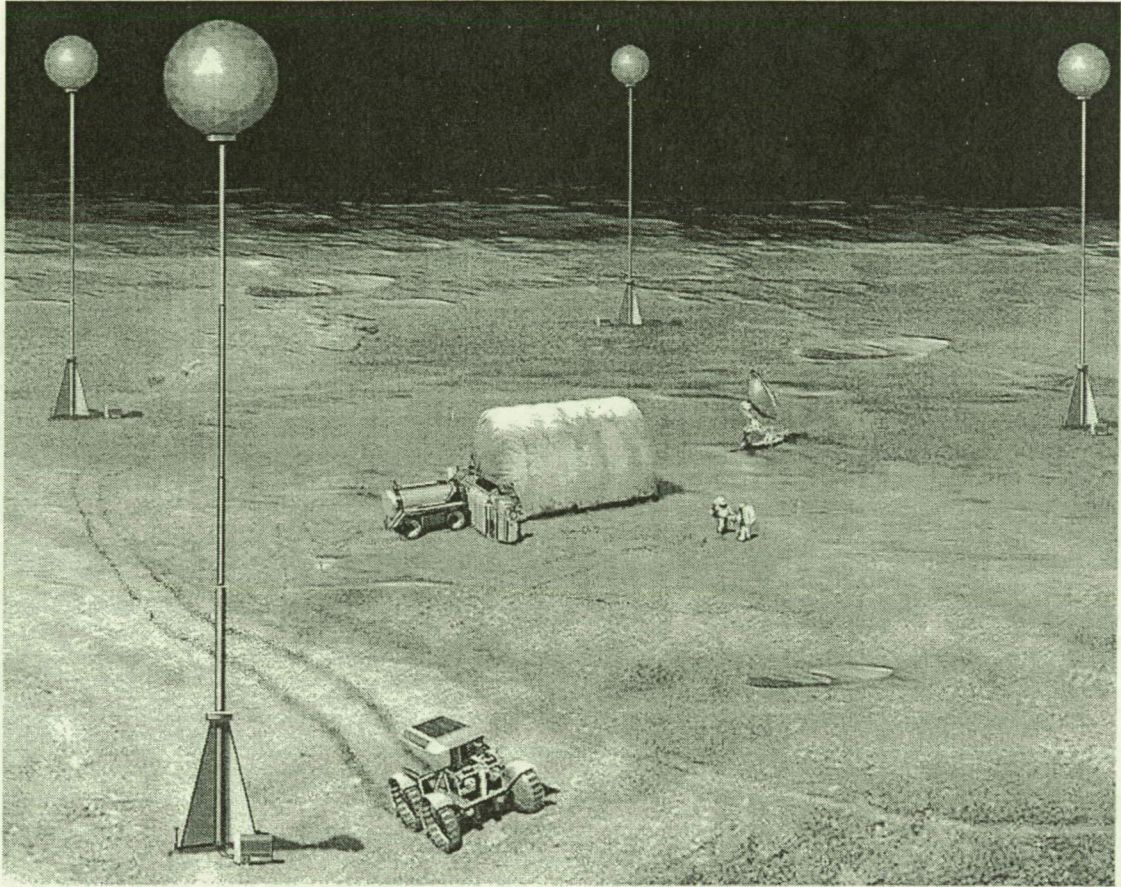


Figure 1: Conceptual electrostatic shield for a moon base from the proposal

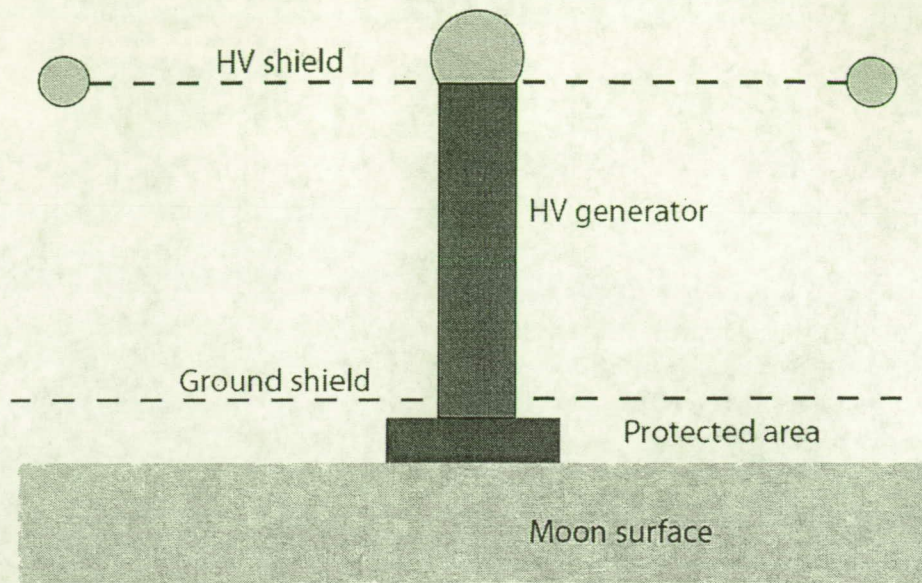


Figure 2: Diagrammatic view – electrostatic shield system for a moon base

single, centralized voltage source (possibly in the form of a black monolith to blend in). For an applied voltage of 20 MV and a conservative gradient of 2.5 MV/m for the vacuum insulators, the generator would rise about 8 m above the ground shield. The high-voltage shield consists of a thin wire netting supported on insulating poles. Voltage grading structures on the outer edge would reduce the chance of breakdown. It may be necessary to cover the central portion of the netting with an opaque material to reduce photoelectron emission on the insulating column.

A larger second net with a negative applied potential would be suspended about 3 m from the surface of the moon. The *ground shield* serves several important functions:

- It reduces the generator load caused by photoelectric emission from the ground.
- It acts as a Faraday cage to protect personnel and equipment from breakdowns and photoemissive charging.
- The shield reduces the field at the moon surface to prevent attraction of dust particles.

Regarding the first item, the significance of photoelectron loading is reviewed in Sect. 3. Section 4 addresses required voltage levels on the ground shield to ensure a net field at the surface that repels electrons.

### 3 Electron photoemission from the lunar surface

A moon base would be exposed to sunlight half the time. The ultraviolet portion of the solar spectrum can generate photoelectrons on the lunar surface as well as on equipment and personnel. Ordinarily the emitting objects would be left with a small positive potential (a few volts) that would attract the low-energy electrons to preserve charge neutrality. Without the ground shield of Fig. 2, the HV electrode would generate a strong attractive field on the lunar surface. In this case, all photo-electrons would travel to the HV shield, loading the voltage generator. Even though the current density may be small, the available emission area is very large. In the configuration discussed in Sect. 5, the area exceeds 3000 m<sup>2</sup>. A related problem is the selective charging of personnel and equipment if their work function differs significantly from the lunar surface. The emission rate from metal equipment could be substantially higher than lunar dirt, resulting in large voltage differences and possibly arcs.

We can make a rough estimate of the available current density to gauge the severity of the problem. First, consider the available photons. Figure 3 plots the integrated solar power flux as a function of photon energy ( $h\nu$ ) in eV. The data were adapted from Ref. [1]. The plotted quantity is the integral of power flux over all higher energies. The second piece of required information is the electron yield as a function of  $h\nu$ . Here, the term *yield* refers to the number of emitted electrons per incident photon. There is considerable variation between materials. Fig. 4 shows data abstracted from Ref. [2] for copper and silicon surfaces, while Fig. 5 shows theoretical predictions for emission from small dust particles from Ref. [3]. It is difficult to make an accurate calculation because the solar spectrum drops rapidly in the energy range of rising emission coefficient. To make a conservative estimate, we take an average yield of  $10^{-3}$  for the portion of the photon spectrum above 6 eV. The photon flux above 6 eV is approximately equal to

$$F_p \cong (0.02 \times 10^{-3}) / (6)(1.6 \times 10^{-19}) = 1.25 \times 10^{14} (\text{photons/s/cm}^2). \quad (1)$$

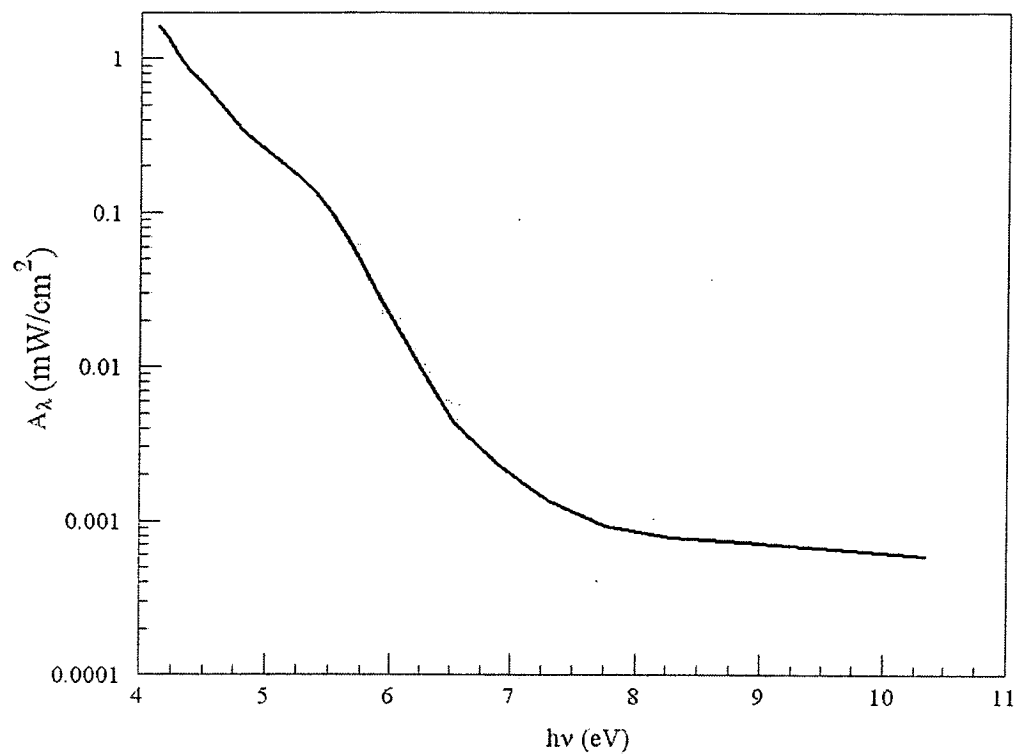


Figure 3: Solar spectrum as a function of photon energy – integral of energy flux from  $h\nu = \infty$ .

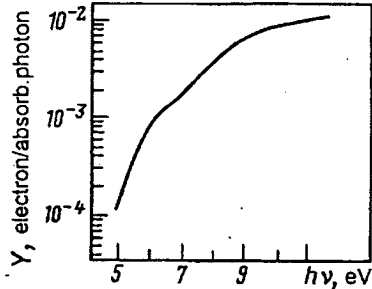


Figure 25.12 PE quantum yield of copper with clean surface [18].

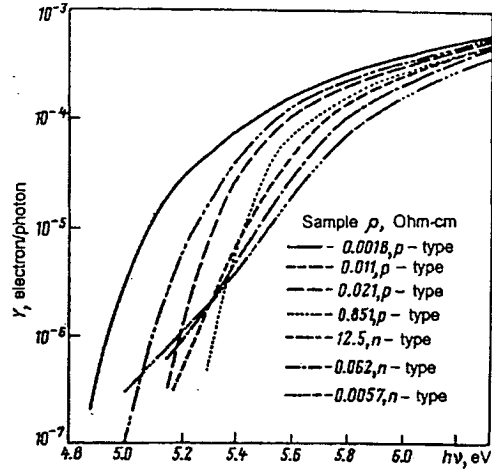


Figure 25.13 PE quantum yield of *n*- and *p*-type silicon with different doping ( $\chi/E_g \approx 4$ ) [16].

Figure 4: Photoelectric yield as a function of photon energy for copper and silicon

The available electron current density is

$$j_e \cong (10^{-3})(F_p)(1.6 \times 10^{-19}) = 2.0 \times 10^{-8}(\text{A}/\text{cm}^2). \quad (2)$$

Multiplying by an area of  $3.0 \times 10^7 \text{cm}^2$  gives a leakage current of 0.6 A.

To maintain voltage, the shield would require a large input power (exceeding 12 MW). Clearly a practical system must include the ground shield of Fig. 2. Photo-emission from the shield can be minimized by using a mesh with high transparency and including a coating with high work function. One remaining problem is the attraction of electrons from the space environment above the HV shield. I will collect data to make estimates in a following report. If there is significant electron current from space, it may be necessary to include an additional ground shield above the HV shield.

## 4 Ground shield design considerations

I envision the ground shield as a high-transparency mesh formed from a square pattern of thin wires. Given the mesh geometry, we must determine the magnitude of negative bias voltage necessary to maintain a repelling electric field at the lunar surface. I set up a simple three-dimensional simulation

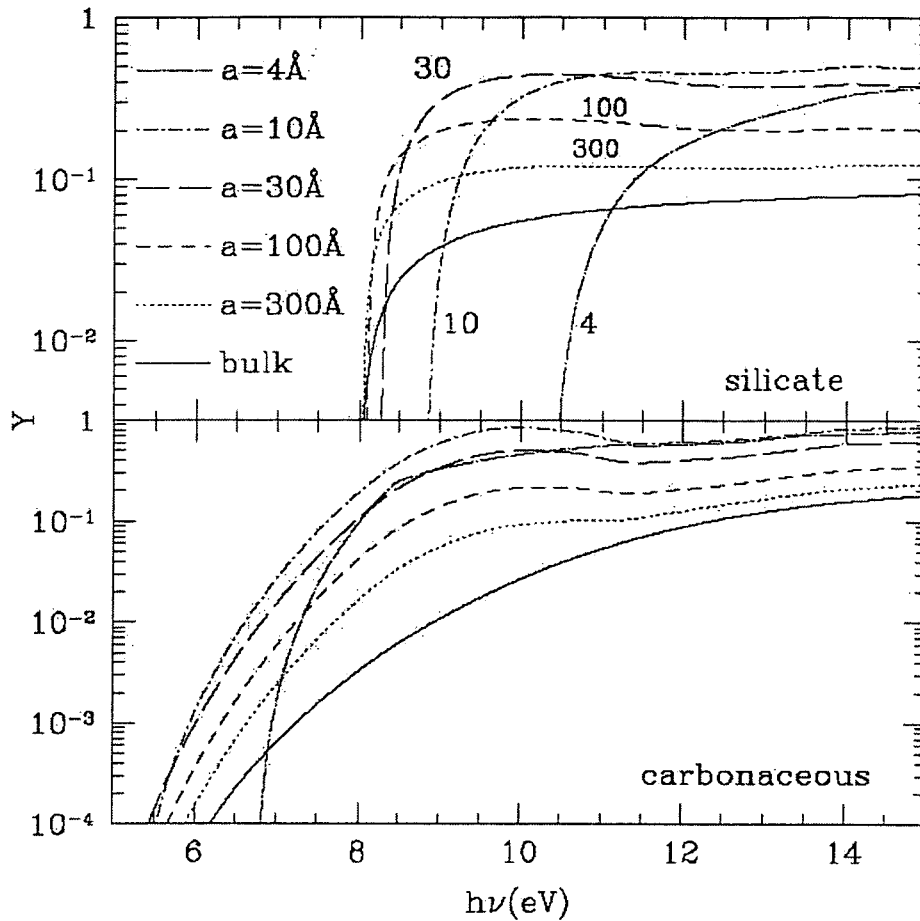


FIG. 5.—Photoelectric yield  $Y$  for neutral graphite and silicate grains as a function of incident photon energy  $h\nu$  for several values of the grain size  $a$ , as indicated.

Figure 5: Photoelectric yield as a function of photon energy for graphite and silicate grains

with the **HiPhi** code to provide the information. The simulation geometry, shown in Fig. 6, consists of an infinite mesh of thin wires in a square pattern with side length  $D$ . A ground plane is located 2 m below the mesh. A plane 2.0 m above the mesh is biased to 5.0 MV to create a gradient  $E_z \cong 2.5$  MV/m. Because of symmetry it was necessary only to model one quadrant of a mesh cell. The Neumann boundary condition ( $\mathbf{E}$  parallel to the surface) was applied on the four sides in the  $x - y$  plane. The shielding effectiveness depends mainly on  $D$  relative to the distance to the ground plane – there is little dependence on the wire diameter. Figure 7 shows calculated equipotential lines near the ground shield in the plane  $y = 0.0$  with  $D = 40.0$  cm and no bias (shield at ground potential). If the wires have diameter  $W = 0.32$  cm (1/8”), the opacity of the mesh is

$$R = \frac{4WD/2}{D^2} = \frac{2W}{D} = 0.032. \quad (3)$$

The field partially penetrates the mesh – the average potential beneath the wire array is about +64 kV. As a result there is an approximately uniform field  $E_z = -33.4$  kV/m in the region between the ground shield and lunar surface, sufficient to extract all photoelectrons. To ensure electron repulsion it would be necessary to apply a bias voltage of about -70 kV to the ground shield. Reducing the wire spacing to  $D = 20$  cm doubles the opacity but significantly reduces the field in the protected region. With a grounded mesh, the field is  $E_z = 6.3$  kV/m, so a bias voltage of about -15 kV would be sufficient. A double-layered ground shield would be desirable for personnel protection. The ideal ground shield system may consist of a grounded mesh at sufficient height to permit operations and a second mesh 1-2 m above with negative voltage to ensure  $E_z$  has a positive value at the lower mesh.

## 5 Shield field configuration and stored energy

I set up a simulation to illustrate the field geometry of a finite-dimension shield system and to calculate the stored electrostatic field energy. I assumed cylindrical symmetry and applied the two-dimensional **EStat** code. Figure 8 shows the simulation geometry. The moon surface at the left is treated as infinite ground plane. The ground shield 2 m above the surface has a 34 m radius and is biased to -60.0 kV. The HV shield 10 m above the surface is biased to +20 MV. The outer radius of the grating electrode is 21 m. I placed

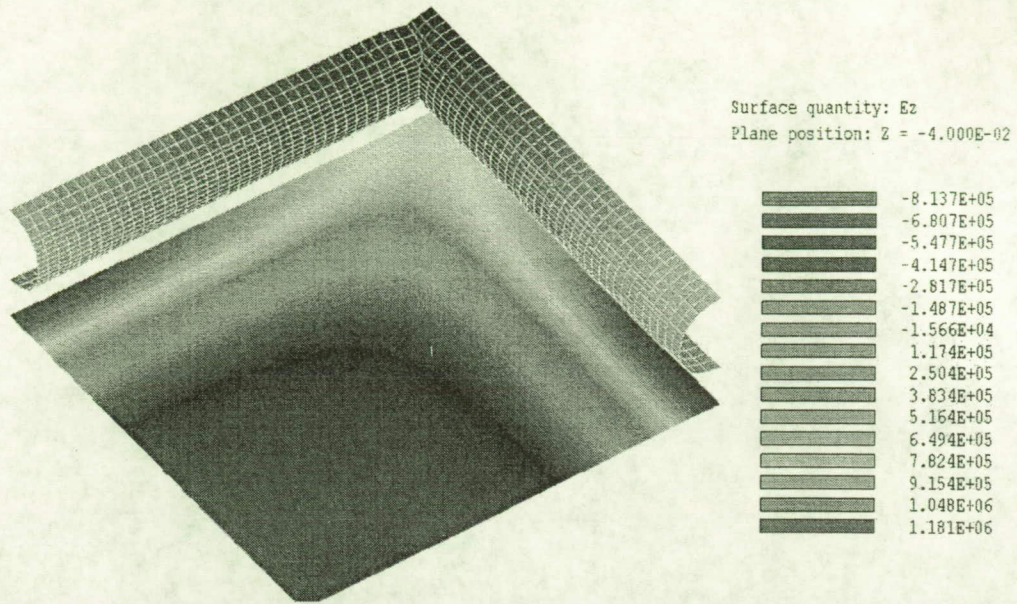


Figure 6: Geometry – **HiPhi** simulation of field penetration of an infinite mesh with wires on a square patten with  $D = 40$  cm. The colored plane 4.0 cm below the wires shows  $E_z$ .

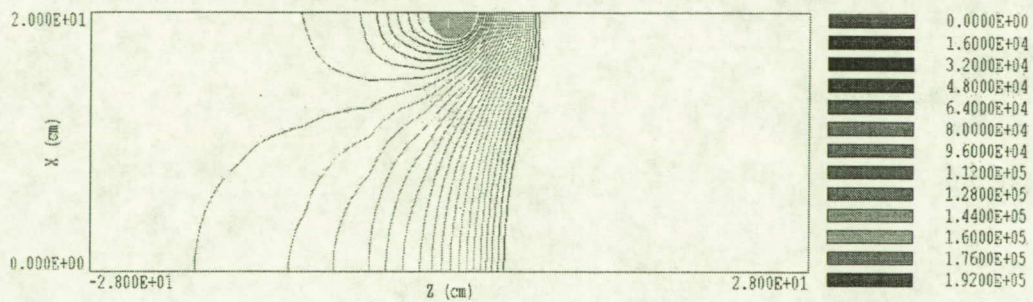


Figure 7: Equipotential lines in the plane  $y = 0.0$  cm near a mesh with  $D = 40$  cm. Ground plane to the left, HV shield to the right.

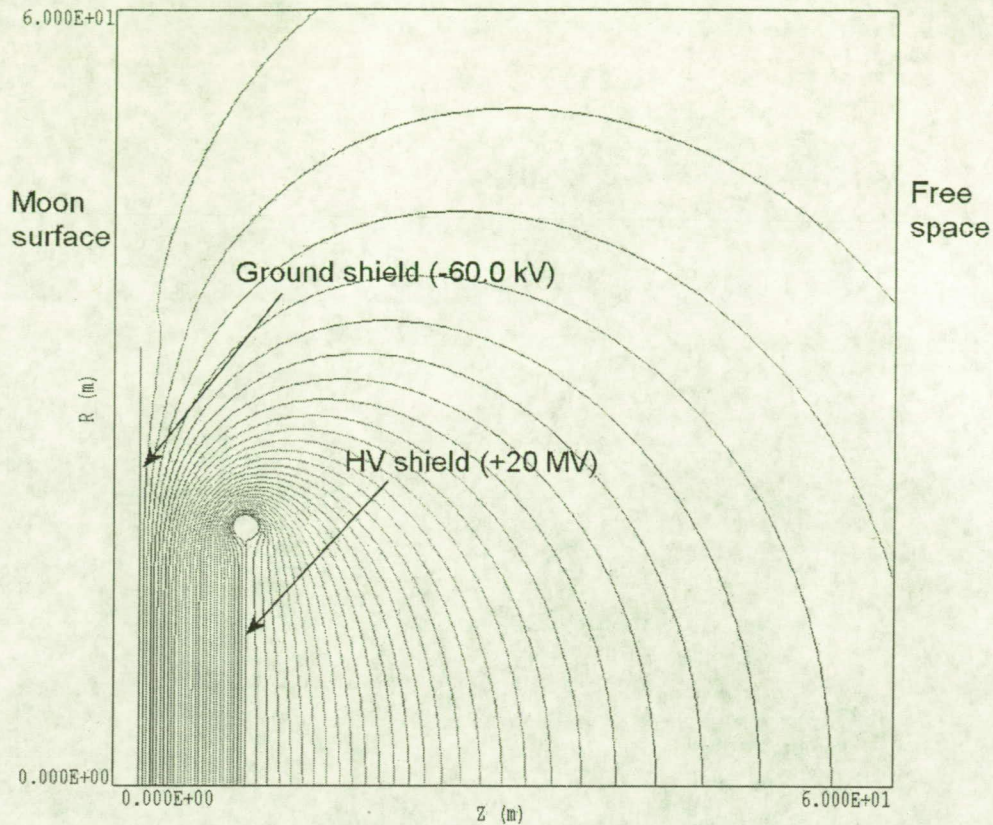


Figure 8: Simulation of a finite-dimensional shield system – geometry and equipotential lines

a grounded boundary at  $z = 100$  m and  $r = 100$  m to represent infinite space. Figure 8 shows calculated equipotential lines – electric fields are normal to the lines. Taking an integral of  $\epsilon_0 E^2/2$  over the solution volume gives a stored electrostatic energy of 0.68 MJ. This amount of energy could cause significant damage in the event of a breakdown, emphasizing the necessity of the ground shield.

The field lines in Fig. 8 have a significant radial extent. Figure 9 shows a scan of  $E_z$  in radius near the lunar surface ( $z = 1.0$  m). The strong negative field values outside the radius of the ground shield could accelerate photoelectrons from a large area. Clearly, the radius of the ground shield must be substantially larger in a practical system.

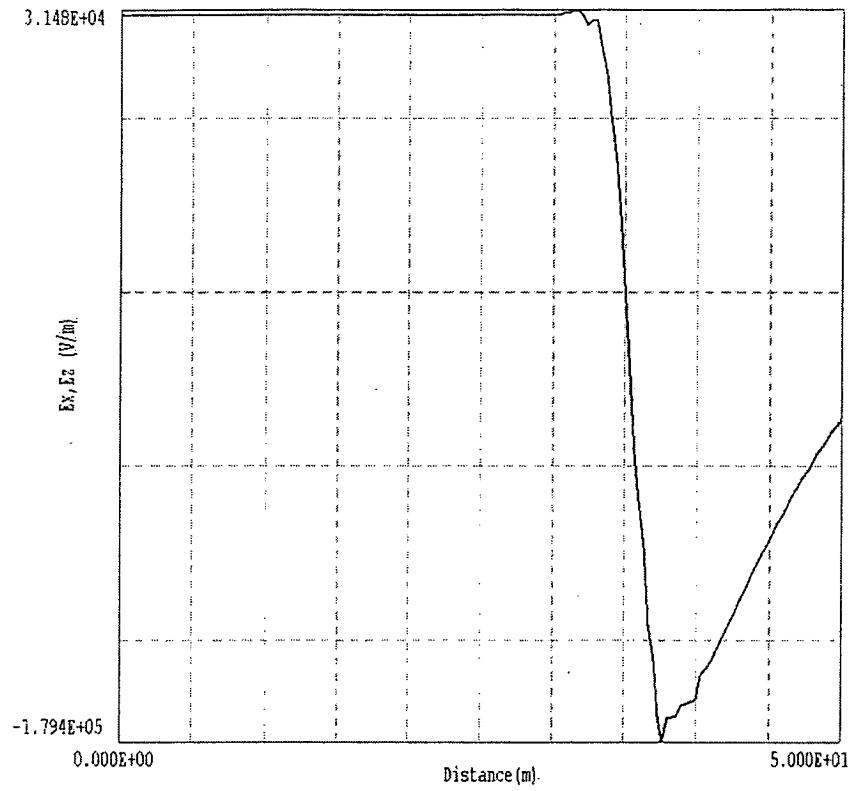


Figure 9: Radial scan of  $E_z$  close to the lunar surface ( $z = 1.0$  m).

## 6 Estimating shield efficiency

I could perform extensive three-dimensional ion orbit calculations to estimate the effectiveness of electrostatic shields of the type of Fig. 2. This effort would be largely unnecessary because it is straightforward to estimate an upper limit on the shield efficiency for all configurations. Because the shield does not change the kinetic energy of penetrating ions, I define the efficiency  $E_s$  as the ratio of the reflected ion flux to the incident flux. For solar proton events which could provide a lethal dose, the quantity  $E_s$  must be close to unity. The following assumptions lead to simple model:

- The incident ions have an isotropic distribution (equal flux per solid angle).
- Ions arrive from free space at the same reference potential as the lunar surface.
- The shield is a plane of infinite transverse extent biased to  $+V_0$ .

Regarding the third condition, finite assemblies like Figs. 1 and 2 have regions with  $\phi < V_0$  and therefore have lower efficiency than the ideal system.

The polar angle  $\theta$  is defined with respect to the z axis in Fig. 8. It equals  $0.0^\circ$  for normal incidence and  $90.0^\circ$  for ions arriving from the horizon. With the assumption of equal flux per solid angle, the normalized probability as a function of angle is given by:

$$p(\theta)d\theta = \sin(\theta)d\theta. \quad (4)$$

Consider a non-relativistic ion incident from  $\infty$  at angle  $\theta$ . The ion has kinetic energy  $T$ , ionization state  $Z_i$  and kinetic energy per unit charge  $T_0 = T/Z_i$ . The component of kinetic energy normal to the lunar surface is

$$T_\perp = T_0 \cos\theta. \quad (5)$$

Because the electric fields are normal to the surface, the condition that the shield reflects an ion is that  $eV_0 \geq T_\perp$ , or  $\cos\theta \leq \cos\theta_0$ , where:

$$\cos\theta_0 = \sqrt{\frac{eV_0}{T_0}} \quad (6)$$

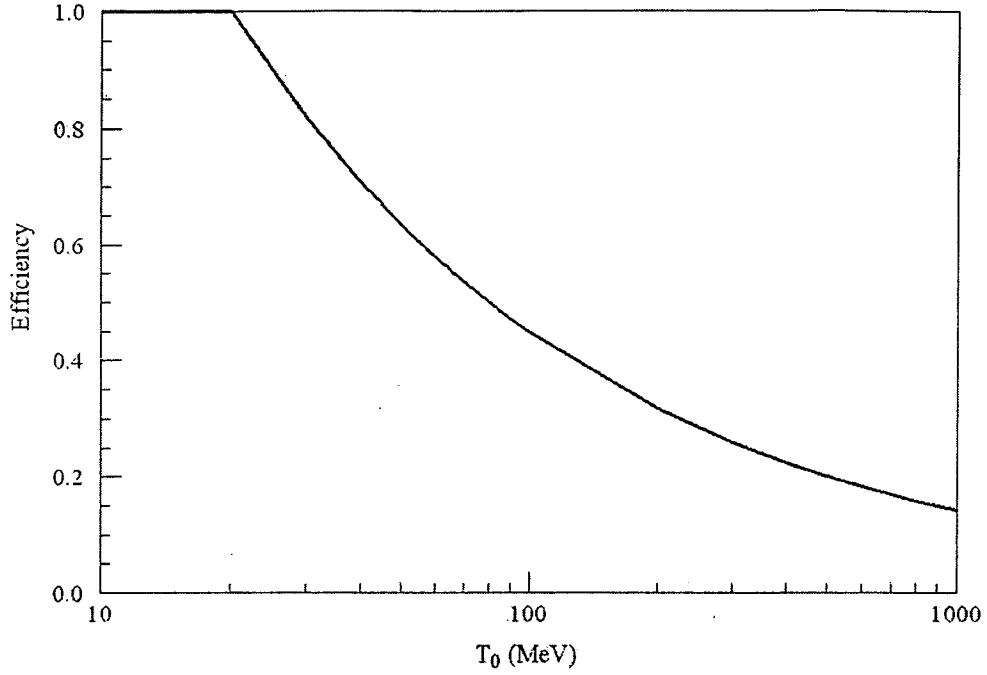


Figure 10: Upper limit on shield efficiency as a function of ion kinetic energy per charge for  $V_0 = 20$  MV

Integrating Eq. 4 from  $\theta = 90.0^\circ$  to  $0.0^\circ$  gives the fraction of reflected ions, equivalent to the shield efficiency:

$$E_s = \int_{\pi/2}^{\theta_0} \sin\theta d\theta = \cos\theta_0 = \sqrt{\frac{eV_0}{T_0}}. \quad (7)$$

To illustrate the implications of Eq. (7), suppose the shield bias is +20 MV. In this case, the shield reflects all ions with kinetic energy per charge  $T_0 \leq 20.0$  MeV. At  $T_0 = 40.0$  MeV, the reflection coefficient is  $E_s = 71\%$ . Figure 10 shows  $E_s$  for the choice  $V_0 = 20.0$  MV over the energy range from  $T_0 = 10.0$  MeV to 1000.0 MeV. Clearly, the shield is ineffective for biological protection from the high-energy flux of gradual solar proton events ( $\sim 100$  MeV) and galactic cosmic radiation ( $\sim 1$  GeV).

## References

- [1] M.P. Thekaekara (ed.), *The Solar Constant and the Solar Spectrum Measured from a Research Aircraft* (NASA Technical Report R-351, Goddard Space Flight Center, Greenbelt, MD).
- [2] T.M. Lifshits and A.I. Musatov, *Electron and Ion Emission*, in **Handbook of Physical Quantities**, I.S. Grigoriev and E.Z. Meilikhov (eds.), (CRC Press, Boca Raton, 1997), 710.
- [3] J.C. Weingartner and B.T. Draine, *Photoelectric emission from interstellar dust – grain charging and gas heating*, *AstroPhy. J.* 134, 263 (2001).